

Prediction of Flow Parameters of Glass Beads-Water Slurry flow through Horizontal Pipeline using Computational Fluid Dynamics

Shofique Ahmed*, Rajesh Arora, Om Parkash

Department of Mechanical Engineering, Amity University Haryana, Gurgaon-122413, India

Received 6 Jun. 2018

Abstract

This paper presents a numerical analysis of two-phase glass beads-water slurry flow based on computational fluid dynamics through a 54.9 mm diameter and 4 m long horizontal pipe considering 125µm glass beads particle size over a flow velocity ranging from 1m/s to 5m/s at various volumetric concentration of the glass beads particle viz. 10%, 20%, 30%, 40% and 50%. For modeling the multiphase flow Eulerian two-phase approach was selected while for modeling the turbulence phase of the flow different turbulence models were introduced and Re-Normalization group K- epsilon model was selected after verifying the robustness of each turbulence model. Structured mesh with non-uniform spacing with a refinement near the wall boundary was selected for discretizing the entire fluid domain while control volume finite difference approach was selected for solving the Navier- Stokes governing equations in Analysis System 14.0 software package. Different flow variables like flow velocity distribution, pressure drop, concentration distribution of the particles, turbulence of the flow and their effects are studied and analyzed. In this study, a generalized mathematical relationship among pressure drop, volumetric concentration and turbulence of the flow has been proposed. The proposed mathematical relationship is then validated against the experimental data available in the previous literature and it was observed that the proposed model can forecast the pressure drop analytically with minimal error. It can be concluded from this study that the solid particles exhibit an asymmetrical distribution pattern along the vertical plane of the pipe cross section. However, as the flow velocity increases the solid particles are observed to be more blended with the liquid and leads to more symmetrical distribution. On the other hand, as the volumetric concentration increases the solid particles experience a more asymmetric distribution pattern and at low flow velocity and high volumetric concentration solid particles are settled at the bottom of the pipe. Volumetric concentration and flow velocity show a direct impact on the pressure drop where the pressure drop rises with the increase in volumetric concentration and flow velocity. Moreover, the comparison of the simulated results proves the practical utility of proposed model and high designing capability of Eulerian-Eulerian model with RNG k-ε turbulence model.

© 2018 Jordan Journal of Mechanical and Industrial Engineering. All rights reserved

Keywords: 3D CFD modeling, Eulerian two-phase model, RNG K-epsilon model, Concentration distribution, Flow velocity distribution, Pressure drop, Slurry pipeline;

Nomenclatures				
Notation	Description	Unit		
α_s	Volumetric concentration of solid	-	Y'	Normalized radial position
α_f	Volumetric concentration of fluid	-	Y	Distance from bottom to top of the pipe along vertical plane
ΔP	Pressure difference	Pa	D	Diameter of the pipe
K_{sf}	Drag coefficient of inter-force	N	L	Length of the pipe
V	Flow velocity of mixture	m/s	Re	Reynolds number
v_s	Flow velocity of solid particles	m/s	ρ	Mass Density
v_f	Flow velocity of fluid	m/s	ρ_f	Mass density for liquid phase
$\bar{\tau}_f$	Stress tensor for fluid phase	N/m ²	ρ_s	Mass density for solid phase
C_{vm}	Coefficient of virtual mass force	N		
C_{vf}	Volumetric concentration of solid particles	-		
C_L	Coefficient of lift	-		
$\mu_{t,f}$	Turbulent viscosity	Pa.s		
k_f	Turbulent kinetic energy	m ² /s ²		
ϵ_f	Turbulent energy dissipation rate	m ² /s ³		
$C(y')$	Predicted concentration distribution of			

1. Introduction

Transportation of solid materials through pipelines has been a common practice over the years in many industries including power generation industries, construction industries, food processing industries, oil and gas, pharmaceutical mining industries chemical industries etc. This mode of transportation of solid materials is preferred to the conventional mode of transportation because it

* Corresponding author e-mail: uddinshofique1991@gmail.com.

reduces environmental hazards, air pollution, less road traffics and more economical. Here solid materials are blended with fluid to form slurry and the slurry is then pumped through the pipeline. There are many terminologies available to classify the slurry flow, but the most frequent categorization is homogenous, heterogeneous, moving bed, stationary bed, and saltation slurry flow regime. Heterogeneous slurry flow regime is the most occurring flow regime among this entire flow regime where the solid particles are heterogeneously distributed in the fluid. The slurry flow through pipeline cannot be considered as pseudo-fluids because the solid particles tend to settle at the pipe bottom; hence it experiences a totally different flow patterns compared to the flow of pure fluid hence it is essential to have a detailed idea about the flow patterns and the behavior of various slurry flow parameters for a better understanding of the slurry flow problems. Many empirical approaches have been developed over the years for a better prediction of the characteristics of various slurry flow parameters. Computational fluid dynamics (CFD) is a sophisticated platform which allows us to explain a wide variety of multiphase flow problems with greater ease and at low cost. Wide range of flow conditions can be solved rapidly which is more or less impracticable with experimental work. It provides a wide range of exclusive clue about the variation of the flow variables inside the flow domain. There are relatively few works on the analysis of slurry flow using CFD technique which gives an exclusive opportunity to the researcher to understand the whole slurry flow process applying CFD technique. Pressure drop, particle flow velocity distribution and the solid particle distributions are the most manipulating flow parameters in a slurry flow process and researchers are aiming for developing a generalized approach to predict the behavior of these flow parameters more precisely since the third decades of the 20th century. Seshadri et. al [1] developed a mathematical correlation which could predict the solid particles distribution in a slurry flow through open channel flow, rectangular ducts and circular pipes. Roco and Shook [2] developed a straightforward algorithm using differential equations for predicting the distribution of solid particles and distribution of particle velocity in a slurry flow containing volumetric concentration less than 40% through pipelines of various pipe diameters. Following their work, Roco and Shook [3] developed a computational model for two-phase analysis of heterogeneous coal-water slurry flow to predict the behaviour of concentration distribution and flow velocity distribution. A two-layer approach was established by Gillies et. al [4] For the analysis of a slurry flow containing coarse particles of coal, gravel and sand and various flow parameters like pressure gradient and concentration distribution of solid particles were precisely predicted using their proposed model; their model was in a good consistency with the data collected from their experimental setup. Gillies and Shook [5] performed a numerical investigation to forecast the pattern of particle concentration distribution in a two-phase solid-fluid slurry flow. Conclusions that were drawn based on their analysis were that the solid particles interaction is limited to the region near the wall boundary and the interaction becomes more spectacular when the particle size becomes larger.

Doron and Berena [6] proposed a three-layer approach for predicting the distribution of particles and pressure gradient in a solid-liquid mixture slurry flow. From their new study they found out that the concentration distribution of the solid particles affects pressure drop. Mukhtar et. al [7] performed an experimental analysis on heterogeneous zinc-iron slurry through long 90° pipe bend. They forecasted the variation of pressure drop in pipe bends at various flow velocity and solid volumetric concentration. Bellus et. al [8] analyzed the pressure gradient of ice slurries containing 5% propylene in water in plate heat exchanger. From their analysis, they concluded that the pressure gradient increases by 15% when volumetric concentration of ice increases from 0% to 20%. Matousek [9] conducted an experimental analysis of sand-water slurry flow through different 35° descending, horizontal and vertical pipes for determining the pressure drop and flow patterns. From their study they found out that pressure drop is lower for smaller sand particles than that of larger sand particles. Also, in vertical pipe the pressure drop is lower than that of horizontal pipe. Scott and Steven [10] studied the slurry flow containing coarse and fine sediments of clay with a varying particle size of the order of 600-2000µm through a horizontal pipeline of 103 mm diameter. The purpose of their work was to examine the effect of concentration of clay on pressure drop and hydraulic gradient. A theoretical model based on genetic algorithm (GA) and support vector regression (SVR) was proposed by Lahiri and Ghanta [11] to forecast the pressure gradient in a solid-liquid slurry flow. Their proposed SVR correlation significantly improved the pressure gradient prediction over an extensive variety of pipe diameters, physical properties and flow conditions. Lahiri and Ghanta [12] proposed a generalized model based on CFD for the prediction of various flow parameters of a slurry flow. Euler-Euler two-phase approach was introduced for modeling the solid-fluid flow and standard K-epsilon approach was used for modeling the turbulence phase of the flow. Using their proposed model, they predicted concentration profile and pressure drop, simulated pressure drop was compared with their experimental data and was in a good consistency. Their investigation showed that pressure gradient is less at low velocity and increases rapidly at high velocity. Chandel et. al [13] conducted an experimental investigation of a slurry flow containing highly concentrated mixture of fly ash and bottom ash and water through a horizontal pipeline. Pressure gradient of the slurry flow was measured from their experiment. Finally, they developed a rheological approach to forecast the pressure gradient and predicted pressure gradient was related with results obtained from experiments and was in a good consistency. Kaushal et al [14] conducted a numerical investigation of slurry flow containing mono-dispersed glass beads particles through horizontal pipeline. Multiphase flow was modelled using Eulerian two-phase model and mixture model while the turbulence phase of the flow was modelled using RNG K-epsilon model. Various flow parameters including pressure drop, velocity distribution and concentration distributions were analyzed in their study. Moreover, they found out that the mixture model is not an appropriate model for predicting the pressure drop correctly while Eulerian model predicts the pressure drop with a higher accuracy.

Nabil et. al [15] anticipated a generalized CFD technique to simulate solid-liquid flow. By using their model, the predicted the behaviour of different flow parameters like velocity distribution and its consequence on pressure gradient considering the influence of the size of particles into concern. From their analysis they concluded that the pressure gradient rises with the rise in concentration as well as pressure gradient rises when the velocity is higher. Kumar et. al [16] conducted a numerical investigation of a slurry flow containing 440 μm diameter sand particles and water through a horizontal pipeline. Eulerian two-phase model and standard K- epsilon model was selected for modeling the flow. From their analysis they predicted the behaviour of pressure gradient, velocity distribution and distribution of solid particles as well as pressure drop was correlated with the data obtained from experiments. Kumar [17] conducted a CFD based numerical simulation of slurry flow consisting of silica sand and water through pipe bends and straight pipes for the prediction of pressure drop. He adopted Eulerian model and K-epsilon model for the analysis. Conclusion from his study was that the pressure gradient rises with flow velocity at pipe bend. Eulerian approach and RNG K-epsilon approach were applied for CFD simulation of sand-water slurry flow through horizontal pipeline by Gopaliya and Kaushal [18]. The pressure drops characteristics along with other flow parameters were predicted in their study.

This current study represents a CFD numerical analysis of Glass beads-water slurry flow through a horizontal pipeline of 54.9 mm diameter and 4m length. Size of the glass beads particles is taken as 125 μm with specific gravity of 2.47. The simulations are conducted over a flow velocity of 1m/s, 2m/s, 3m/s, 4m/s and 5m/s at solid particle volumetric concentration of 10%, 20%, 30%, 40% and 50%. Eulerian two-phase approach was selected for modeling the multiphase flow while different turbulence models were introduced, and their robustness was verified. It was found that RNG K-epsilon turbulence approach is the most suitable for modeling the turbulence phase of the flow. A mathematical correlation was developed and validated for the analytical prediction of pressure drop over flow velocity at different volumetric concentration. Finally, the simulated outcome of pressure gradient was correlated with the experimental pressure drop available in the work of Kaushal and Tomita [19].

2. Mathematical model

Selection of proper mathematical model plays a significant character in modeling the flow problems in a numerical analysis. Slurry flow contains solid and fluid phase thus it is a multiphase flow problem. CFD software package allows the selection of various multiphase models like discrete phase, mixture and Eulerian multiphase model for the modeling of the complex multiphase flow. Slurry flows not being a dilute phase flow problem; usage of discrete phase model is restricted for modeling its flow. Kaushal et. al [14] suggested that the mixture model cannot determine the pressure gradient of a slurry flow accurately, hence based on their study Eulerian two-phase model is adopted in this present study. In this study, the solid particles were assumed to be mono-dispersed. In other words, the solid particles were assumed to behave

like liquid particles because of its dispersed nature. Moreover, the granular version of Eulerian model is preferred to the non-granular version because unlike non-granular version, it considers the collision and friction among the solid particles which is essential for slurry flow. For modeling the turbulence phase of the flow several turbulence models were introduced in this present study and their robustness was determined, it was found that the RNG K-epsilon approach is the best suited model for modeling the turbulence phase of this slurry flow problem.

2.1. Eulerian model

The Eulerian model cannot differentiate solid-fluid and fluid-fluid multiphase flows. In Eulerian model, it is assumed that the slurry flow comprises separate fluid and solid phases, and they structure a continuum, so that the volume concentration of solid (α_s) and fluid (α_f) is equal to 1. i.e. $\alpha_s + \alpha_f = 1$. This model satisfies both law of conservation of momentum and mass for solid and liquid individually. The forces that act on a single fluid particle are:

- Static pressure gradient, ΔP .
- Inertial force caused by interaction of particles or solid pressure gradient ΔP_s .
- Difference in velocity between the solid and fluid phase causes the drag force, $K_{sf}(\vec{v}_s - \vec{v}_f)$ where, K_{sf} is the drag coefficient of inter-force, where \vec{v}_f the velocity of fluid is phase and \vec{v}_s is the velocity of solid phase.
- Forces due to viscosity, $\nabla \cdot \bar{\tau}_f$, $\bar{\tau}_f$ is being the stress tensor for fluid phase.
- $\rho \vec{g}$, is the body force.
- Virtual mass force, $C_{vm} \alpha_s \rho_f (\vec{v}_f \nabla \vec{v}_f - \vec{v}_s \nabla \vec{v}_s)$ where, C_{vm} is the coefficient of virtual mass force and is taken as 0.5 in this current work.
- Lift force, $C_L \alpha_s \rho_f (\vec{v}_f - \vec{v}_s) \times (\nabla \times \vec{v}_f)$, where, C_L is the coefficient of lift, taken as 0.5 in this current work.

2.2. Governing equations

The Continuity and Momentum equations are formulated as [14]

Continuity Equation

$$\nabla \cdot (\alpha_t \rho_t \vec{v}_t) = 0, \text{ t being either solid or fluid} \quad (1)$$

Momentum Equation for fluid phase

$$\nabla \cdot (\alpha_f \rho_f \vec{v}_f \vec{v}_f) = -\alpha_f \nabla P + \nabla \cdot \bar{\tau}_f + \alpha_f \rho_f \vec{g} + K_{sf}(\vec{v}_s - \vec{v}_f) + C_{vm} \alpha_f \rho_f (\vec{v}_s \cdot \nabla \vec{v}_s - \vec{v}_f \cdot \nabla \vec{v}_f) + C_L \alpha_s \rho_f (\vec{v}_f - \vec{v}_s) \times (\nabla \times \vec{v}_f) \quad (2)$$

Momentum Equation for solid phase

$$\begin{aligned} \nabla \cdot (\alpha_s \rho_s \vec{v}_s \vec{v}_s) = & -\alpha_s \nabla P - \nabla P_s + \nabla \cdot \bar{\tau}_s + \alpha_s \rho_s \vec{g} \\ & + K_{sf}(\vec{v}_f - \vec{v}_s) \\ & + C_{vm} \alpha_s \rho_f (\vec{v}_f \cdot \nabla \vec{v}_f - \vec{v}_s \cdot \nabla \vec{v}_s) \\ & + C_L \alpha_s \rho_f (\vec{v}_s - \vec{v}_f) \times (\nabla \times \vec{v}_f) \quad (3) \end{aligned}$$

2.3. Turbulence model

The turbulent model is solved using RNG K- ϵ model along with other additional conditions causing interfacial turbulent momentum transfer. The fluid phase Reynolds stress tensor is given by:

$$\overline{v_{t,f}} = -\frac{2}{3}(\rho_f k_f + \mu_{t,f} \nabla \bar{v}_f) \bar{I} + \mu_{t,f} (\nabla \bar{v}_f + \nabla \bar{v}_f^{tr}) \quad (4)$$

Here $\mu_{t,f}$ is the viscosity corresponding to turbulence. An analytical differential interrelationship for turbulent viscosity is provided with RNG K- ϵ model for modeling the flow at lower Reynolds number. At large Reynolds number (which is the case in current study) this analytical correlation converts to:

$$\mu_{t,f} = \rho_f C_\mu \frac{k_f^2}{\epsilon_f} \text{ With } C_\mu = 0.09 \quad (5)$$

The prediction of turbulent kinetic energy k_f and turbulent energy dissipation rate ϵ_f by Standard K- ϵ and RNG K- ϵ approach is almost very much alike. Standard and RNG k - ϵ approach differ in such a fashion that RNG k - ϵ approach contains a supplementary expression in the ϵ equation:

$$R_\epsilon = \frac{C_\mu \rho \eta^3 (1 - \eta/\eta_0) \epsilon^2}{(1 + \beta \eta^3) k} \quad (6)$$

Where, $\eta = Sk/\epsilon$, $\eta_0 = 4.38$, $\beta = 0.012$, the constant parameters are taken as $C_{\mu m} = 0.0845$, $C_{1\epsilon} = 1.42$, $C_{2\epsilon} = 1.68$, $C_{3\epsilon} = 1.3$, $\sigma_k = 0.75$, $\sigma_\epsilon = 1.2$

2.4. Wall functions

Wall functions are collections of empirical and semi-empirical formulae that yield a better solution near the wall boundary of a flow domain. In this study due to the presence of higher gradient terms the near wall boundary of the flow domain demands a special treatment during the simulation. This can be obtained by selecting standard wall functions accessible with the RNG K- ϵ model.

3. Numerical Solution

3.1. Geometry and mesh

A circular pipe of 4 m length and 54.9 mm diameter is modeled in ANSYS workbench design modular which defines the computational flow domain for this slurry flow problem. Structured hexa core elements with non-uniform spacing have been selected for discretizing the flow domain using multizone method. Seven inflation layers with smooth transition size of 0.05 mm and growth ratio of 1.2 has been introduced for refining the mesh size near the boundary wall. The generated mesh contains approximately 200901 elements.

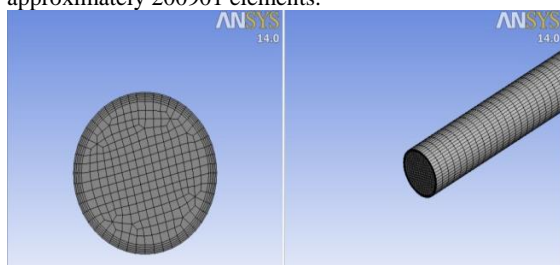


Figure 1. 2D and 3D view of generated mesh

3.2. Boundary conditions

Three faces enclosing the flow domain has been introduced namely outlet boundary, wall boundary and inlet boundary. Values are specified at those boundary conditions to initiate the flow through the flow field. Details of the boundary condition are shown in Table 1.

Table 1: Types of boundary conditions applied to the flow domain.

Boundary location	Boundary type	Turbulence (specification method)
Inlet	Fluid phase: velocity inlet in Z direction Solid phase: velocity inlet in Z direction and volumetric concentration $\alpha_s = C_{vf}$	Turbulent intensity=3.5% Hydraulic diameter=0.0549
Wall	No slip boundary condition for fluid phase Full slip boundary condition for solid phase	-
Outlet	Fluid phase: pressure outlet Solid phase: pressure outlet	Turbulent intensity=3.5% Hydraulic diameter=0.0549

3.3. Solution strategy and convergence criteria

In this current work, the Navier-Stokes governing equations are solved in FLUENT 14.0 software package. Finite difference control volume approach was selected for discretizing momentum and mass equations. Momentum equation, turbulent kinetic energy and turbulent dissipation rate are discretized with second order upwind scheme and volumetric concentration is discretized with first order upwind scheme. For pressure and velocity coupling phase coupled SIMPLE algorithm is selected. Convergence of problem depends on the scaled residual. For this flow problem the residuals contain continuity, X-velocity, Y-velocity, Z-velocity for both the phases; k and ϵ for fluid phase and volumetric concentration for solid phase which need to be converged at some specific region. Application of these schemes confirmed better stability, accuracy and convergence of the flow problem. Moreover, decreasing the value of under relaxation factors ensured better convergence of the problem. URF (under relaxation factor) for volumetric concentration has been reduced to 0.3 from 0.5 and for momentum it has been reduced from 0.7 to 0.5.

3.4. Grid independency test

In every numerical analysis it is highly recommended to select an optimal mesh for the analysis of flow patterns and flow parameters with higher accuracy. In this study a grid independency test is introduced where five mesh with different number of elements viz. 95000, 150000, 201000, 310000 and 387000 are introduced. Using this mesh, the problem has been simulated applying same boundary conditions (velocity=5 m/s and $C_{vf}=0.5$) for all mesh and velocity profile is drawn for each mesh. Plots of the outcome are shown in figure 2.

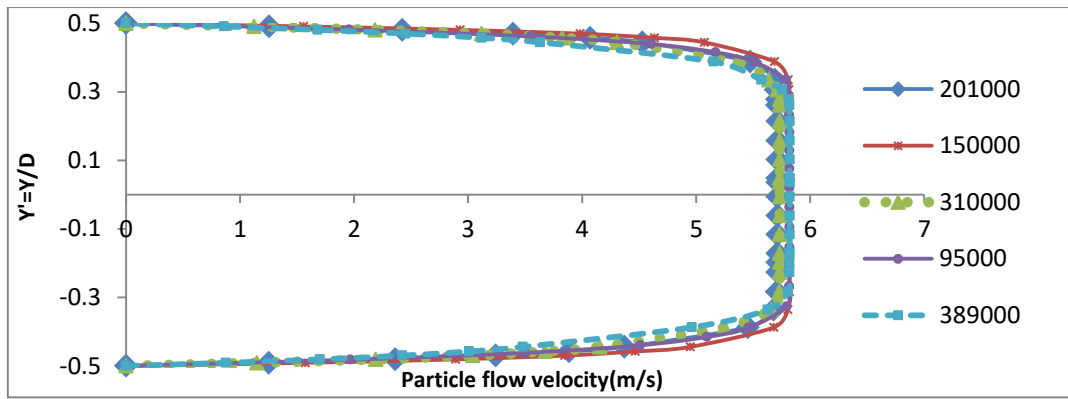


Figure 2. Velocity distributions for different mesh at $V = 5\text{m/s}$ and $C_{vf} = 0.5$

It is confirmed from figure 2 that the velocity profile of the mesh containing 201000 elements and the mesh containing 310000 elements are super imposing with each other. So, the mesh containing 201000 elements has been considered as optimal mesh and it is used for the final calculation in this present study.

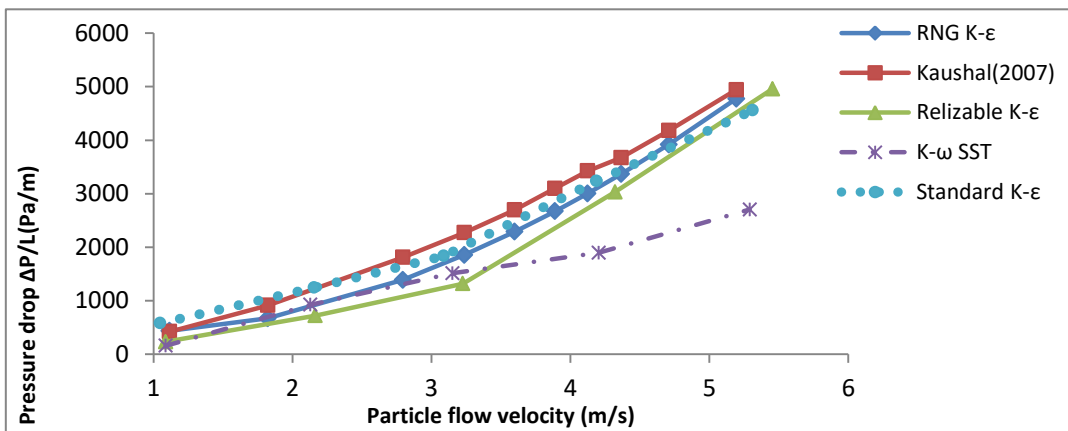


Figure 3. Comparison of experimental and simulated pressure drop at $C_{vf} = 0.3$ using different turbulent model.

3.5. Validation of turbulence model

The turbulence model of this slurry flow is validated with data obtained from the experiments obtainable in the work of Kausal and Tomita [26]. For validating the model, several test simulation runs are carried out using RNG K-epsilon model, Standard K-epsilon model; Realizable K-epsilon model and K-omega SST model along with Eulerian two-phase approach to investigate the precision of these turbulence models in forecasting the experimental pressure drop data. From figure 3, it can be noticed that the RNG K-epsilon turbulence model is the most robust model in forecasting the pressure drop compared to other turbulence model thus confirming the validity of the simulation model.

The simulation matrix used in performing the simulation in this study is shown in table 2 where RNG K-epsilon model along with Eulerian two-phase model are adopted for all the simulation.

4. Results and discussions

4.1. Concentration profile of solid phase

This section shows the simulated values of solid volumetric concentration along a vertical centerline of the pipe cross section at the outlet. $C(y')$ is the predicted solid

particles concentration distribution along the pipe cross section at the outlet, C_{vf} is the volumetric concentration of solid particles, which can be computed as the mean value over the length of the chord in Y direction, mathematically presented as below:

$$C_{vf} = \frac{1}{2y} \int_{-y}^{+y} \alpha_s(y, Y') dy \quad (7)$$

Where $Y' = Y/D$, Y is the height of the vertical centerline from bottom to top of the pipe cross section in Y-direction.

Table 2. Description of simulation parameters used in this study.

Simulation parameters	Values
Pipe diameter (D)	0.0549 m
Pipe length (L)	4 m (> 50D)
Size of glass beads particle (D_p)	125 μm
Particle Solid volumetric concentration	0.1 to 0.5 (10% to 50%)
Specific gravity of particle	2.47
Specific gravity of water	1.00
Velocity of mixture	1m/s to 5m/s
Turbulence equation	RNG K-epsilon
Multiphase model	Eulerian two-phase model

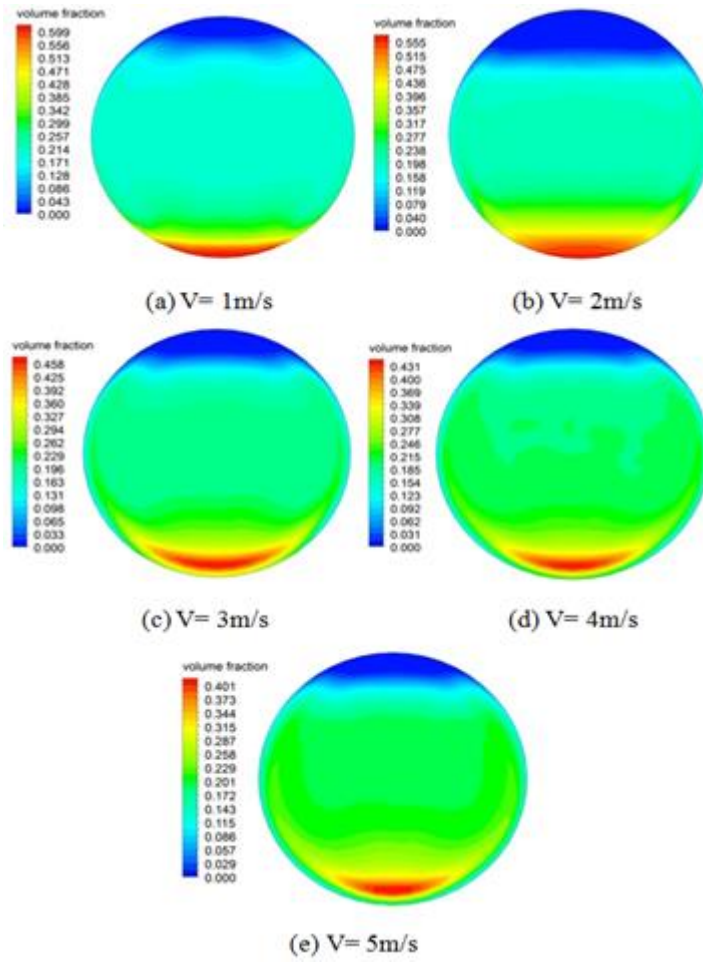


Figure 4. Solid concentration distribution α_s predicted at $C_{vf}=0.2$

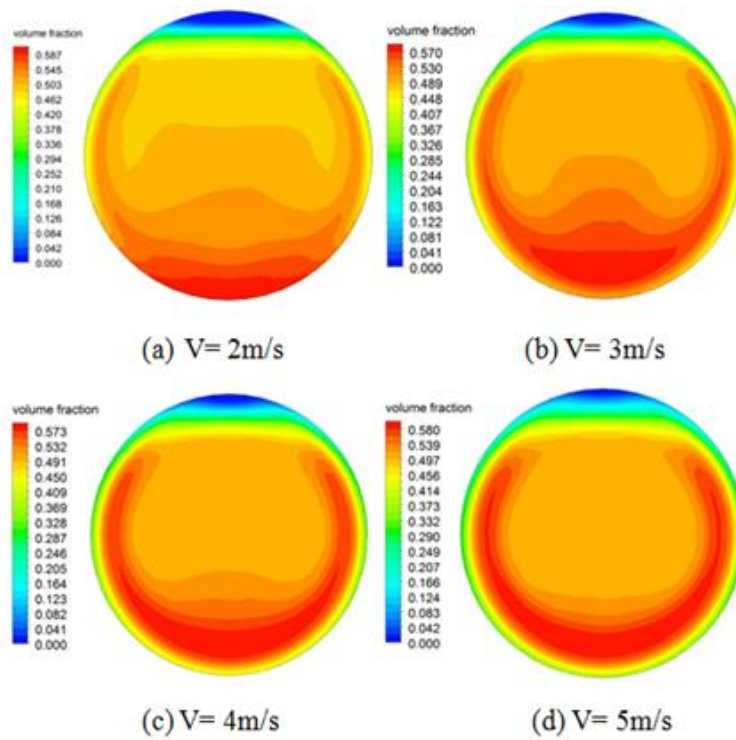


Figure 5. Solid concentration distribution α_s predicted at $C_{vf}=0.5$

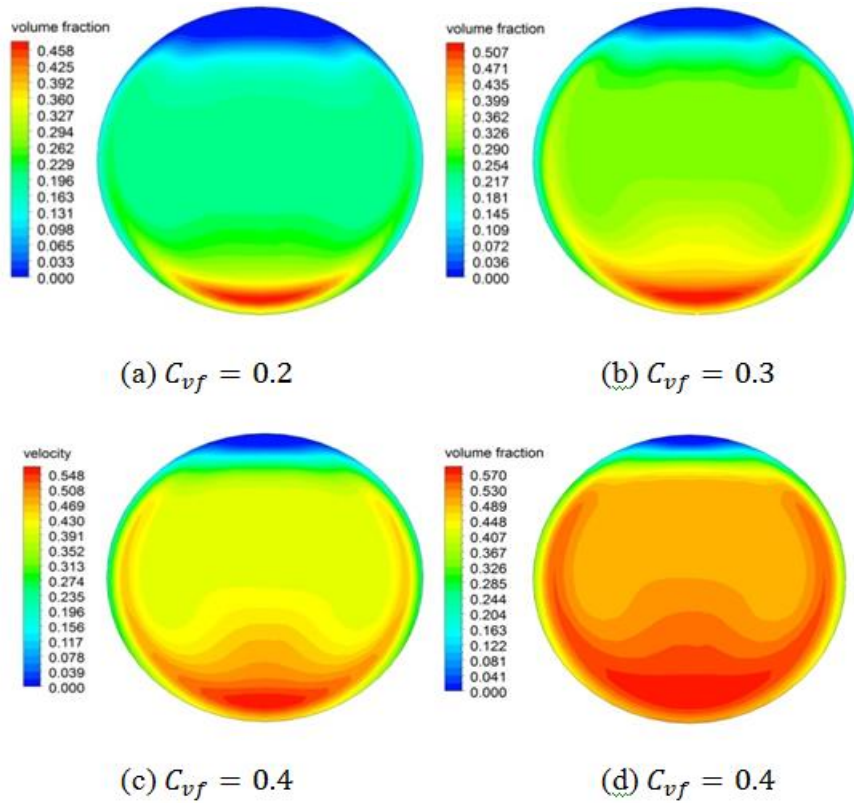


Figure 6. Solid concentration distribution α_s predicted at $V=3\text{m/s}$ for different volumetric concentration.

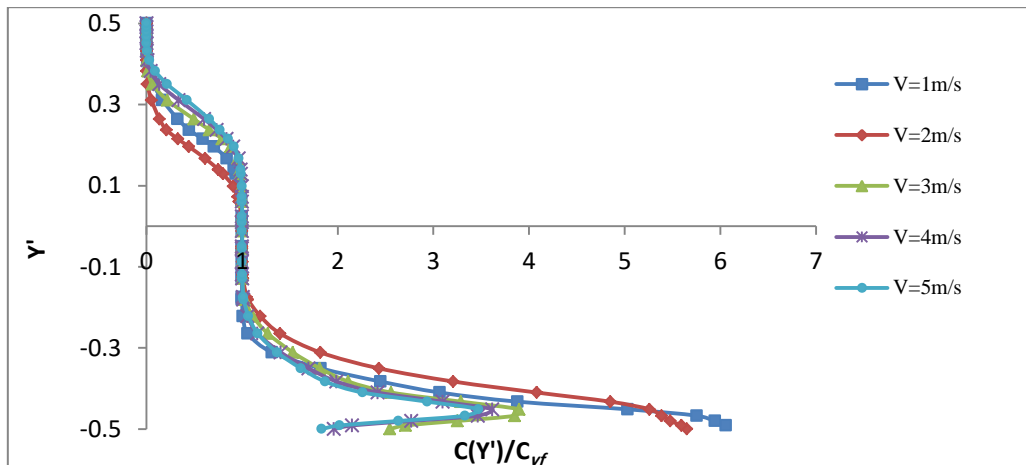


Figure 7. Plots of predicted solid concentration $\alpha_s(-y, y)$ at $C_{vf} = 0.1$

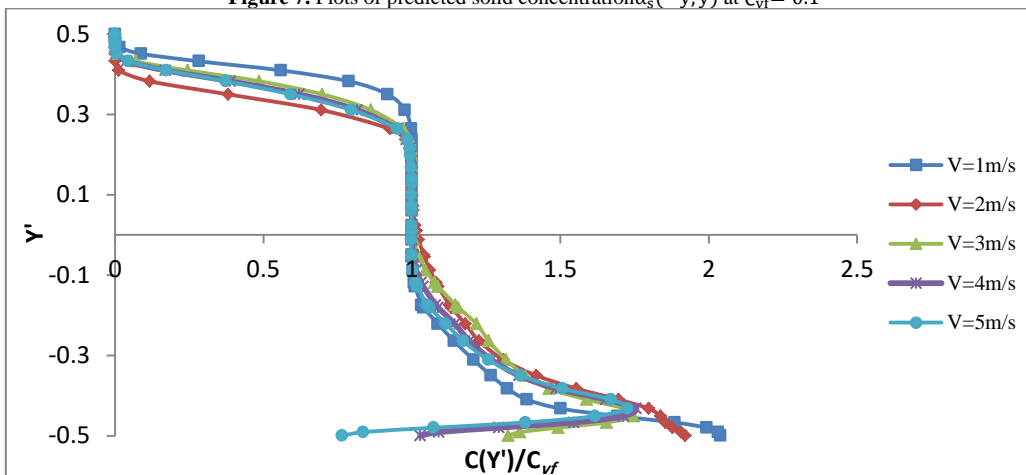


Figure 8. Plots of predicted solid concentration $\alpha_s(-y, y)$ at $C_{vf} = 0.2$

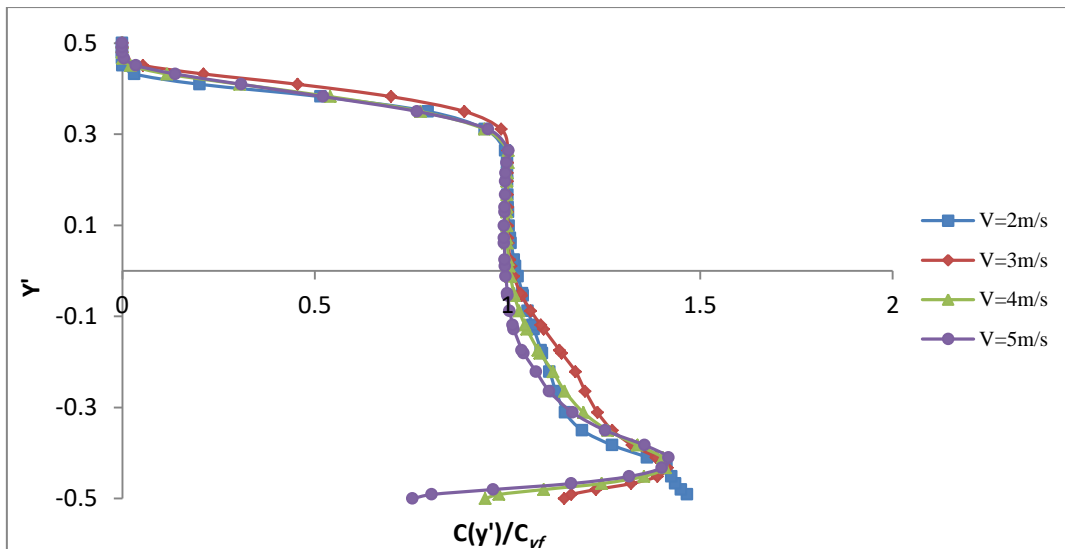


Figure 9. Plots of predicted solid concentration $\alpha_s(-y, y)$ at $C_{vf} = 0.3$

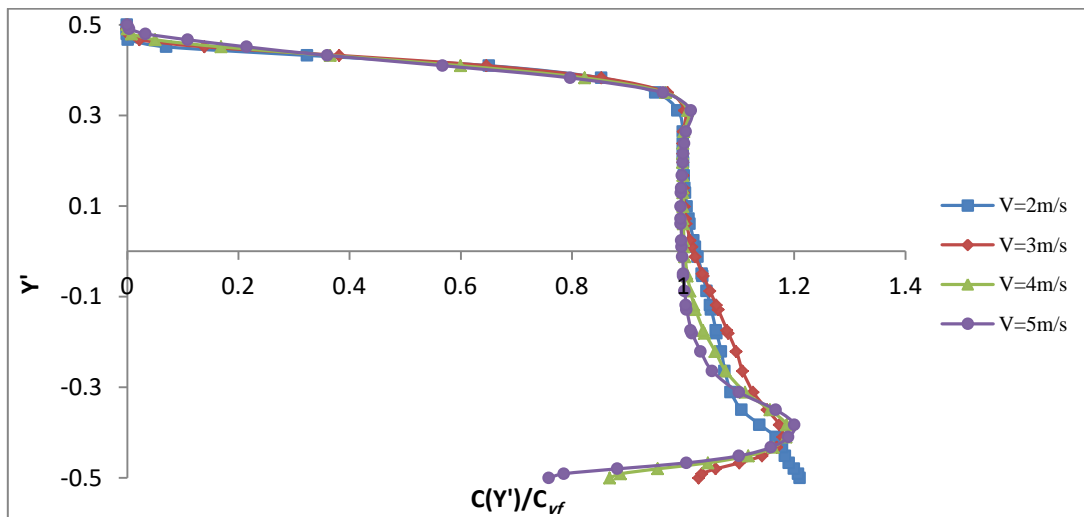


Figure 9. Plots of predicted solid concentration $\alpha_s(-y, y)$ at $C_{vf} = 0.4$

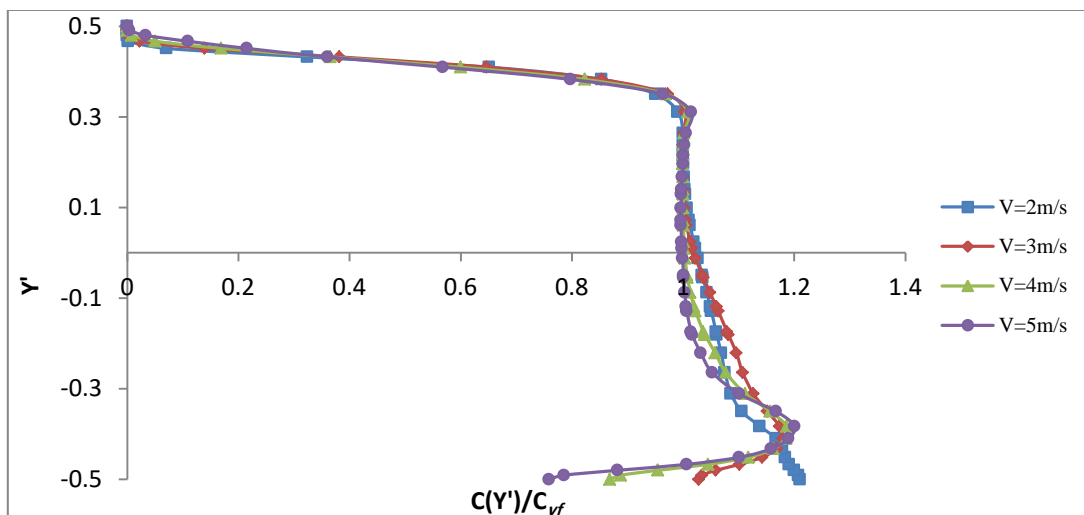


Figure 10. Plots of predicted solid concentration $\alpha_s(-y, y)$ at $C_{vf} = 0.5$

4.1.1. Effect of particle flow velocity and volumetric concentration of solid particles on concentration distribution of solid particles

It may be examined from figure 4 to 10 that solid particles distribution shows an asymmetrical nature along the vertical plane and the solid particles are likely to accumulate at the pipe base because of effect of gravitation and the high concentration zone is established at the base of the pipe. It is noteworthy that for each constant volumetric concentration as the flow velocity increases the particles become more buoyant and suspended in the fluid rather than settling down at the pipe bottom, this is because of the reason that with the rise in velocity the turbulence of the flow becomes high which is accountable for the buoyancy of solid particles. Furthermore, the contact of solid particles with the pipe wall becomes more visible at higher flow velocities [Refer Figure 4, 5, 7, 8, 9, 10]. It may also be noticed that when the volumetric concentration raises for each constant flow velocity the distribution of solid particles become more symmetric across the horizontal plane [Refer Figure 6]. This is because at high volumetric concentration turbulence of the flow increases, thereby providing a complete mixing of the solid particles with the fluid; yielding a more symmetrical particle distribution across the horizontal plane.

4.1.2. Effect of volumetric concentration of solid particles on turbulence of the flow

Figure 11 illustrates the impact of solid volumetric concentration on turbulence of the flow (Reynolds number) at a constant flow velocity viz. 1m/s, 3m/s, 4m/s and 5m/s respectively. It can be observed that at a given flow velocity the turbulence of the flow becomes higher with the rise in solid volumetric concentration. This happens because as the solid volumetric concentration rises, there is a raise in particle-particle, particle-fluid and particle-wall contacts. Moreover, at high concentration the solid particles try to gather more at the pipe bottom thereby blocking a part of

effective flow area, which causes an increase in flow velocity and hence turbulence increases.

4.2. Velocity profiles

Figure 12 to 17 demonstrate the distribution of particle flow velocity $v_{sz}(x, y)$ at solid volumetric concentration (C_{vf}) of 0.3, 0.4 and 0.5 respectively. $v_{sz}(x, y)$ is the Z component of the velocity perpendicular to the cross section of the pipe (X-Y plane). The velocity contours are obtained at the outlet of the pipe.

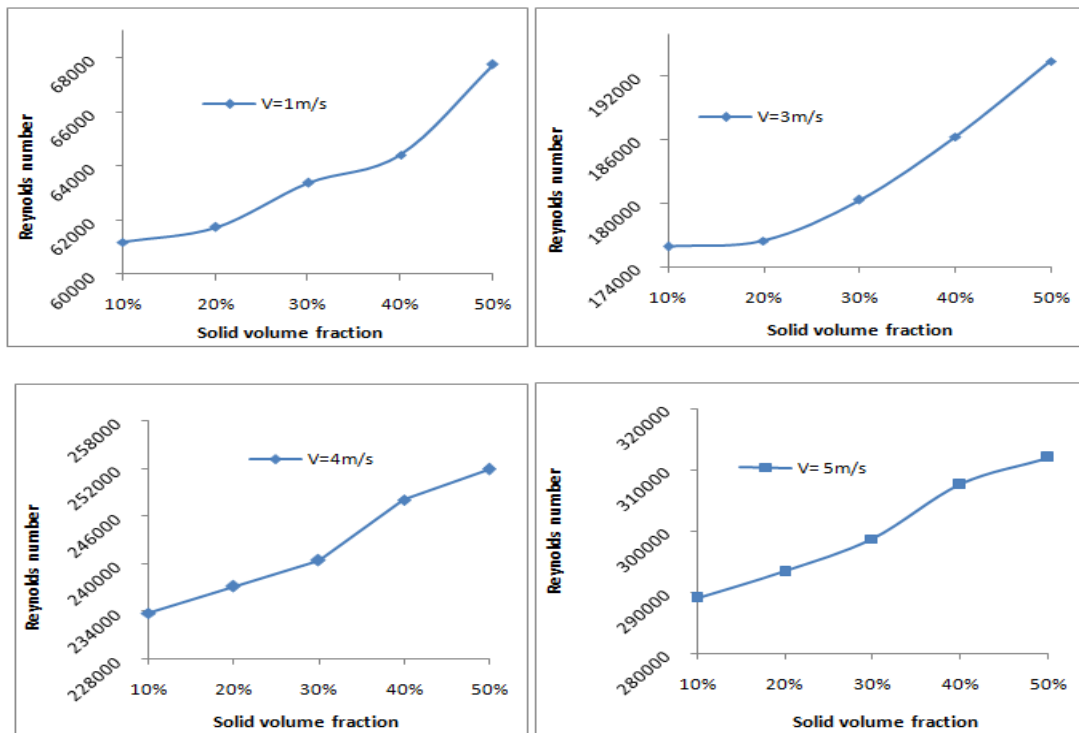


Figure 11. Plot of effects of solid volumetric concentration on turbulence of the flow.

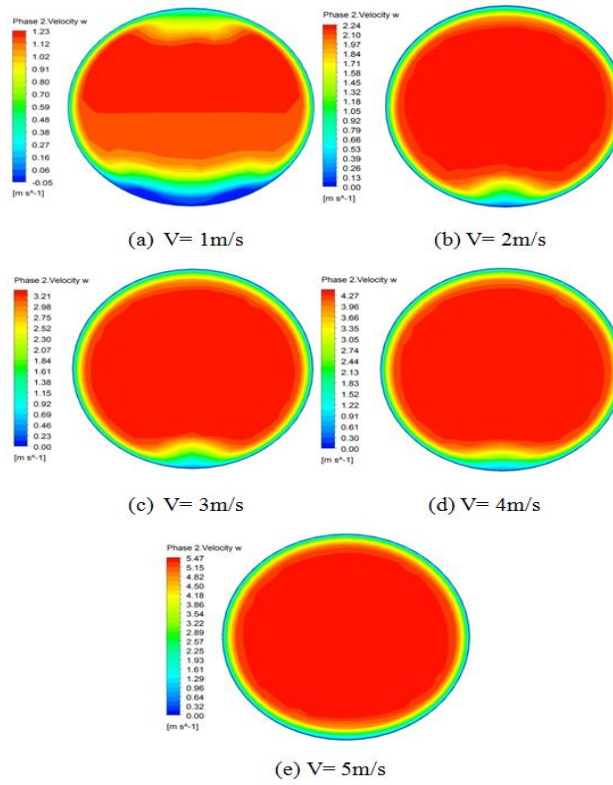


Figure 12. Simulated velocity distribution $v_{sz}(x, y)$ at $C_{vf} = 0.3$

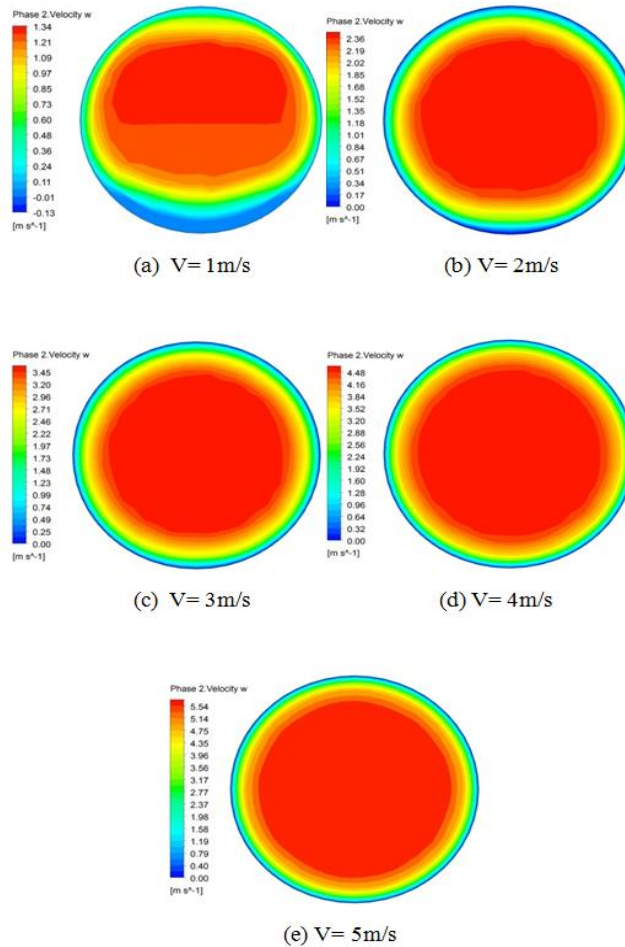


Figure 13. Simulated velocity distribution $v_{sz}(x, y)$ at $C_{vf} = 0.5$

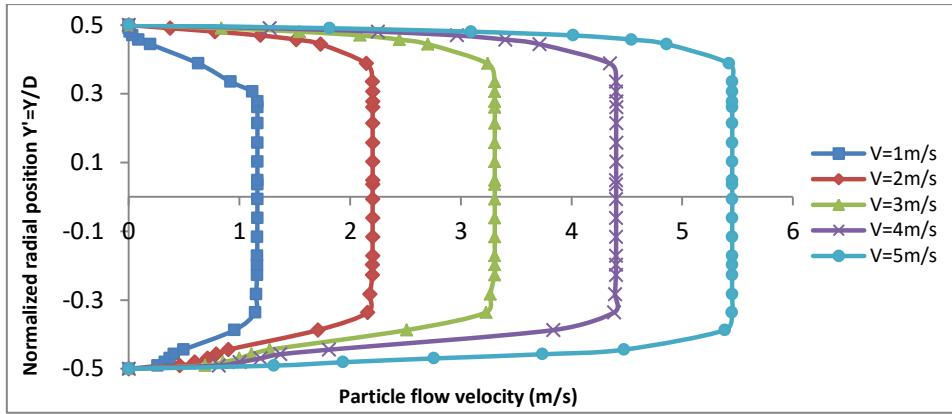


Figure 14. Plots of simulated velocity distribution $v_{sz}(x, y)$ at $C_{vf} = 0.3$

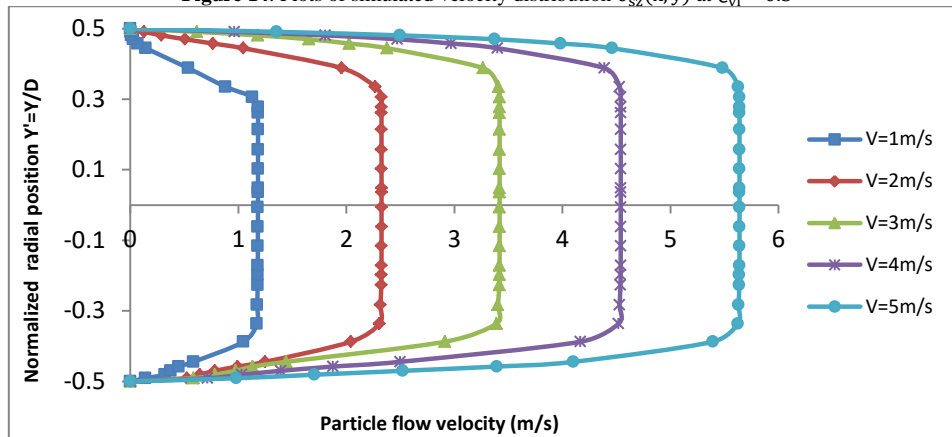


Figure 15. Plots of simulated velocity distribution $v_{sz}(x, y)$ at $C_{vf} = 0.4$

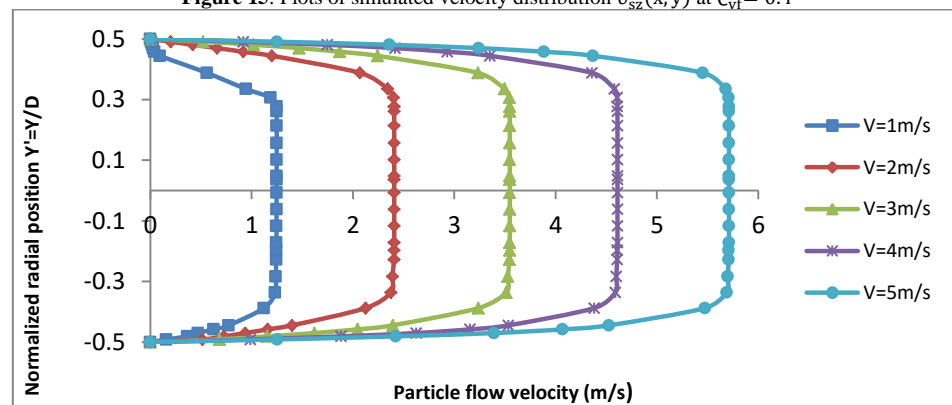


Figure 16. Plots of simulated velocity distribution $v_{sz}(x, y)$ at $C_{vf} = 0.5$

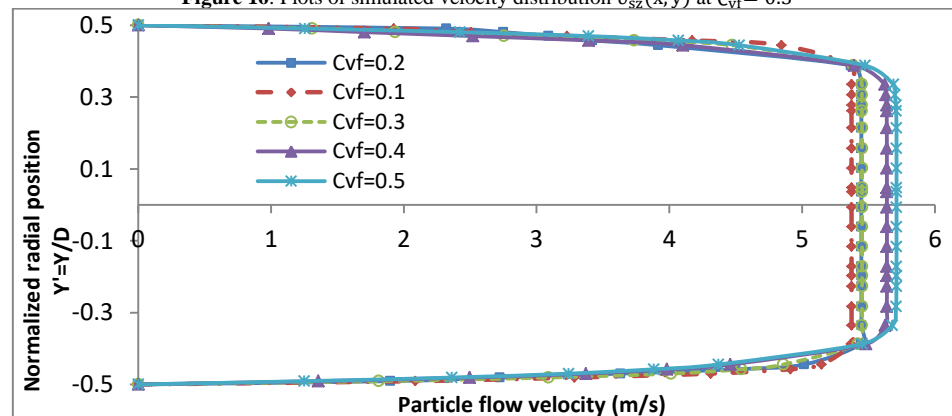


Figure 17. Plot of simulated flow velocity distribution of solid particles at given velocity $V=5\text{m/s}$ and different solid volumetric concentration level.

4.2.1. Effect of solid volumetric concentration on particle flow velocity

From figure 12 to 16 it can be monitored that the solid velocity distribution is parabolic and asymmetrical in the base section of the pipe at low velocities ($V= 1\text{m/s}, 2\text{m/s}$) due to larger shear force, as the particles are likely to accumulate at the pipe bottom owing to gravitational effect. However, the solid velocity distribution appears to be more symmetrical as the velocity increases ($V=5\text{ m/s}$). This happens because as velocity and solid volumetric concentration increases there is an increase in Reynolds number (turbulence) which provides a complete blending of fluid and solid particles, the solid particles no longer seem to be accumulated at the base of the pipe, accordingly distribution of particle flow velocity turns into more symmetric.

Figure 17 explains the allocation of particle flow velocity alongside vertical centerline of the pipe cross section from top to bottom at a given velocity viz. 5 m/s at different solid volumetric concentration level. From this figure, a remarkable change in velocity distribution can be observed. For a given velocity, as the volumetric concentration of solid particles raises the velocity distribution becomes more symmetric and the flow velocity increases. This is because of the reason that an increase in solid volumetric concentration causes rise in turbulence and hence rise in particle flow velocity.

4.3. Pressure drop

4.3.1. Effect of solid volumetric concentration on pressure drop

Figure 18 shows the impact of solid volumetric concentration on pressure drop. It is noteworthy that at a constant flow velocity the pressure gradient rises with the surge in solid volumetric concentration. This is because the rise in solid volumetric concentration causes an increase in turbulence of the flow (Reynolds number). Pressure drop is directly proportional to Reynolds number. Hence with the rise in solid volumetric concentration, the pressure drop increases. Moreover, it can be observed that at higher velocities the degree of rise in pressure drop is more.

4.3.2. Effect of turbulence of the flow (Reynolds number) on pressure drop

Figure 19 illustrates the influence of turbulence on pressure gradient at different solid volumetric concentration. It is noteworthy that the pressure drop rises with a raise in turbulence (Reynolds number). Moreover, it also may be scrutinized that as the solid volumetric concentration rises the degree of increase in pressure drop also increases. This is because Reynolds number raises with a rise in solid volumetric concentration.

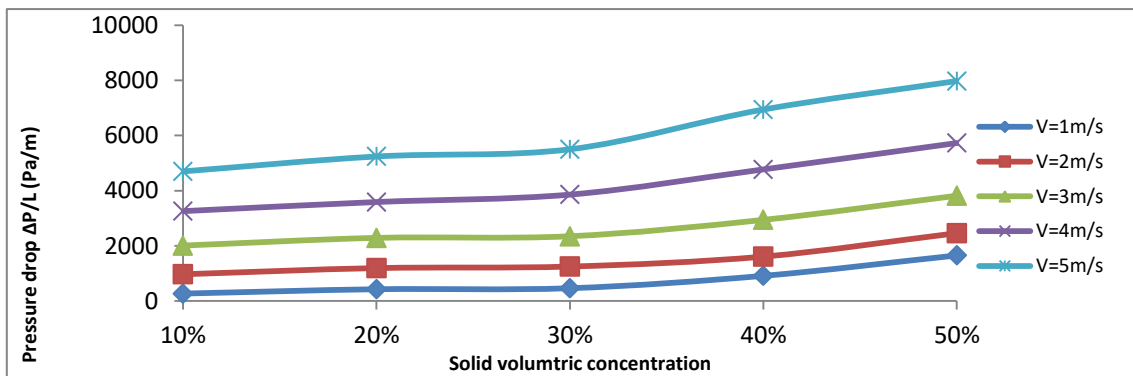


Figure 18. Plots of the effect of solid volumetric concentration on pressure drop at different flow velocity.

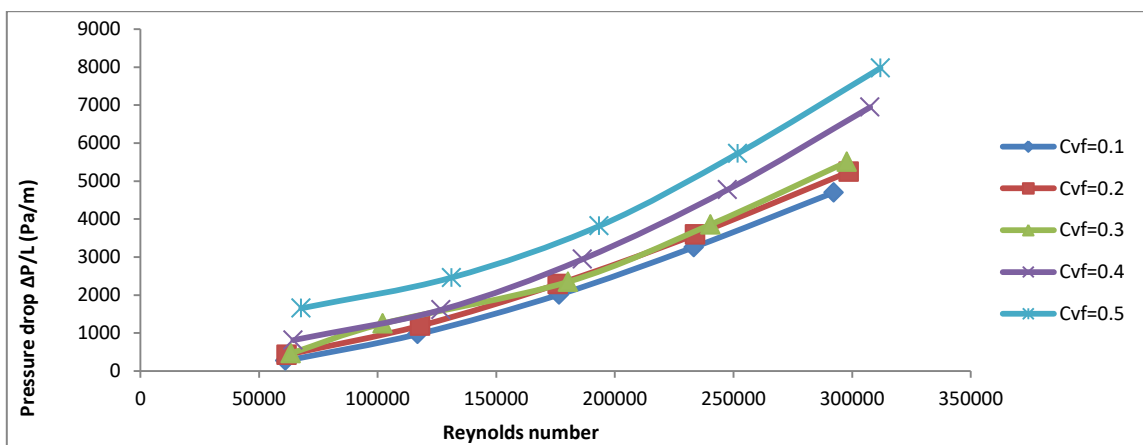


Figure 19. Plots of effect of Reynolds number on pressure drop at different solid volumetric concentration.

4.3.3. Mathematical relationship for pressure drop in terms of turbulence and solid volumetric concentration

The impact of turbulence on pressure gradient is discussed in section 4.3.2. A mathematical correlation is developed for analytical calculation of the influence of turbulence on pressure drop. Initially a polynomial graph was plotted for pressure drop with Reynolds number to predict the functional correlation between them. Then all data variation of pressure drop at different solid volumetric concentrations was plotted against Reynolds number (figure 19). The mathematical model is represented as

$$\frac{\Delta P}{L} = A(Re)^2 + B(Re) + C \tag{8}$$

Where, $\frac{\Delta P}{L}$ is the pressure drop.

Re is Reynolds number.

A, B and C are constants.

Table 3. Values of constants for equation (8) at different solid volumetric concentration

Solid volumetric concentration (C _{vf})	Values of constant A	Values of constant B	Values of constant C
C _{vf} = 0.1	3 × 10 ⁻⁸	0.008	-307
C _{vf} = 0.2	4 × 10 ⁻⁸	0.007	-250
C _{vf} = 0.3	5 × 10 ⁻⁸	0.006	+17.5
C _{vf} = 0.4	6 × 10 ⁻⁸	0.001	+426.4
C _{vf} = 0.5	7 × 10 ⁻⁸	0.000	+950

The effect of solid volumetric concentration on Reynolds number is discussed in the section 4.1.2. A mathematical correlation has been developed for the analytical calculation of the influence of solid volumetric concentration on Reynolds number. Initially an exponential graph has been plotted for the Reynolds number with solid volumetric concentration to establish the functional correlation between them. Then all information variation of Reynolds number at different velocities is plotted against solid volumetric concentration (figure 11). The developed mathematical relationship is represented as:

$$Re = \alpha(\beta e^{nC_{vf}}) \tag{9}$$

Where, Re is the Reynolds number.

C_{vf} is the volumetric concentration of solid particles. α, β and n are constants and their values at different velocities are enlisted in the following table 4

Table 4. Values of constants for equation (9) at different velocities.

Flow velocity	Values of α	Values of β	Values of n
V= 1m/s	59125	1.00	0.246
V= 2m/s	59125	1.857	0.3
V= 3m/s	59125	2.835	0.234
V= 4m/s	59125	3.586	0.193
V= 5m/s	59125	4.383	0.2

Combination of equation 8 and equation 9 yields a generalized form of mathematical correlation for the analytical prediction of pressure drop with different flow velocities at various solid volumetric concentration levels. Combining the two equations we get,

$$\frac{\Delta P}{L} = A(Re)^2 - B(Re) + C \tag{10}$$

Where, $Re = \alpha(\beta e^{nC_{vf}})$

The values of constants are enlisted in table 3 and 4.

Equation 10 confirms that the pressure drop is a function of Reynolds number and solid volumetric concentrations, represented as:

$$\frac{\Delta P}{L} = F_n\{Re, C_{vf}\} \tag{11}$$

4.3.4. Verification of the proposed mathematical relationship

For finding the accuracy and robustness of the developed mathematical correlation a test case is considered where pressure drop is calculated for different flow velocities at solid volumetric concentration of 0.1 to 0.5. This calculated result is then compared with the experimental result of pressure drop available in the literature [26]. Calculated results and the experimental results are enlisted in table 6 to 9. Initially from equation 9 Reynolds number at concentration level 0.1 to 0.5 for flow velocity of 1m/s to 5m/s is calculated. The results are displayed in table 5.

Table 5. Values of Reynolds number at different solid volumetric concentration for various flow velocities.

Velocity	Reynolds number at				
	C _{vf} = 0.1	C _{vf} = 0.2	C _{vf} = 0.3	C _{vf} = 0.4	C _{vf} = 0.5
V= 1m/s	60597	62106	63653	65238	66863
V= 2m/s	113712	117176	120744	124421	128210
V= 3m/s	172458	176541	180721	185000	189380
V= 4m/s	217250	221484	225800	230200	234684
V= 5m/s	265721	271089	276565	282152	287852

Now from the equation 8 pressure drop at different Reynolds number for velocity range of 1m/s to 5m/s at solid volumetric concentration of 0.1 to 0.5 are calculated and the results are displayed in table 6 to 9

Table 6: Comparison of calculated and experimental pressure drop at C_{vf} = 0.1

Reynolds number at C _{vf} = 0.1 for	Calculated Pressure drop (Pa/m)	Experimental pressure drop(Pa/m)	Average error (%)
V=1m/s	60597	287.93	3.19%
V=2m/s	113712	990.6	
V=3m/s	172458	1964.91	
V=4m/s	217250	2846.92	
V=5m/s	265721	3936.99	

Table 7. Comparison of calculated and experimental pressure drop at C_{vf} = 0.2

Reynolds number at C _{vf} = 0.2for	Calculated Pressure drop (Pa/m)	Experimental pressure drop(Pa/m)	Average error (%)
V=1m/s	62106	339.03	4.41%
V=2m/s	117176	1119.44	
V=3m/s	176541	2232.45	
V=4m/s	221484	3262.59	
V=5m/s	271089	4587.19	

Table 8. Comparison of calculated and experimental pressure drop at $C_{vf} = 0.4$

Reynolds number at $C_{vf} = 0.4$ for		Calculated Pressure drop (Pa/m)	Experimental pressure drop (Pa/m)	Average error (%)
		for $C_{vf} = 0.4$	for $C_{vf} = 0.4$	
V=1m/s	65238	746.99	717.181	3.86%
V=2m/s	124421	1479.65	1343.56	
V=3m/s	185000	2664.9	2378.46	
V=4m/s	230200	3836.12	3935.34	
V=5m/s	282152	5485.13	5741.88	

Table 9. Comparison of calculated and experimental pressure drop at $C_{vf} = 0.5$

Reynolds number at $C_{vf} = 0.5$ for		Calculated Pressure drop (Pa/m)	Experimental pressure drop (Pa/m)	Average error (%)
		for $C_{vf} = 0.5$	for $C_{vf} = 0.5$	
V=1m/s	66863	1262.94	1593.22	2.338%
V=2m/s	128210	2071	2090.4	
V=3m/s	189380	3435	3118.64	
V=4m/s	234684	4766.62	4655.37	
V=5m/s	287852	6691	6621.47	

The results of pressure drop calculated by the proposed mathematical relationship and experimental pressure drop can be plotted as follows:

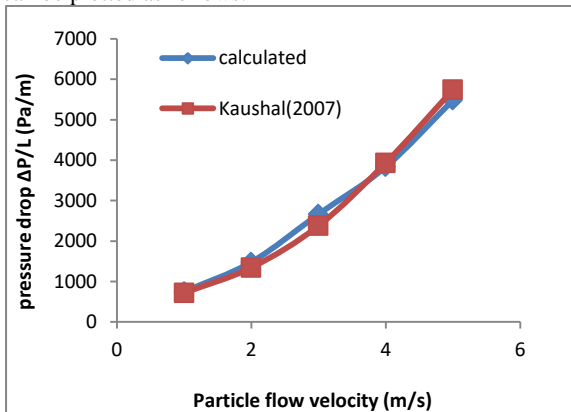


Figure 20. Comparison of calculated and experimental pressure drop at $C_{vf} = 0.1$

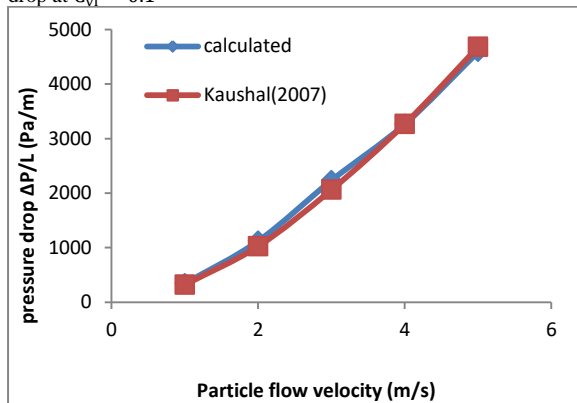


Figure 21. Comparison of calculated and experimental pressure drop at $C_{vf} = 0.2$

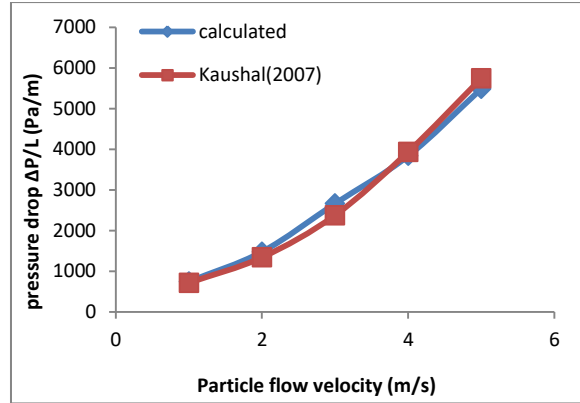


Figure 22. Comparison of calculated and experimental pressure drop at $C_{vf} = 0.4$

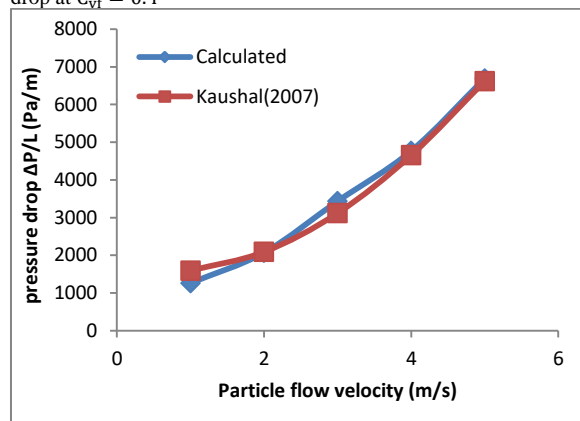


Figure 23. Comparison of calculated and experimental pressure drop at $C_{vf} = 0.5$

From table 6 to 9 and figure 20 to 23 it can be examined that the calculated pressure drop over flow velocity at solid volumetric concentration of 0.1, 0.2, 0.4 and 0.5 show an excellent conformity with the pressure drop data obtained from experiments available in the work of Kaushal and Tomita [26]. It can be concluded that the proposed mathematical relationship shows robustness and accuracy in analytical calculation of the pressure drop. The average percentage error of this correlation is found to be 3.449%.

4.3.5. Validation of the study

The intention of this work is to validate the simulated results

of the pressure drop over flow velocity at various solid volumetric concentrations with the experimental results of pressure drop available in the work of Kaushal and Tomita [19].

Figure 24 shows the impact of particle flow velocity on pressure drop at different solid volumetric concentration. Differential pressure along the length ($\Delta P/L$) is taken on Y-axis and particle flow velocity has been taken on X-axis for plotting the graphs. For comparing the simulated and experimental results, Plot digitizer software is used to extract the coordinates from the experimental results. The proposed investigations can also be carried out for the optimization of performance parameters of other systems like Brayton, Stirling heat engines etc. Further, the optimum value of pressure drops with the application evolutionary algorithms on these pipeline systems is the foremost need of this era [20-37].

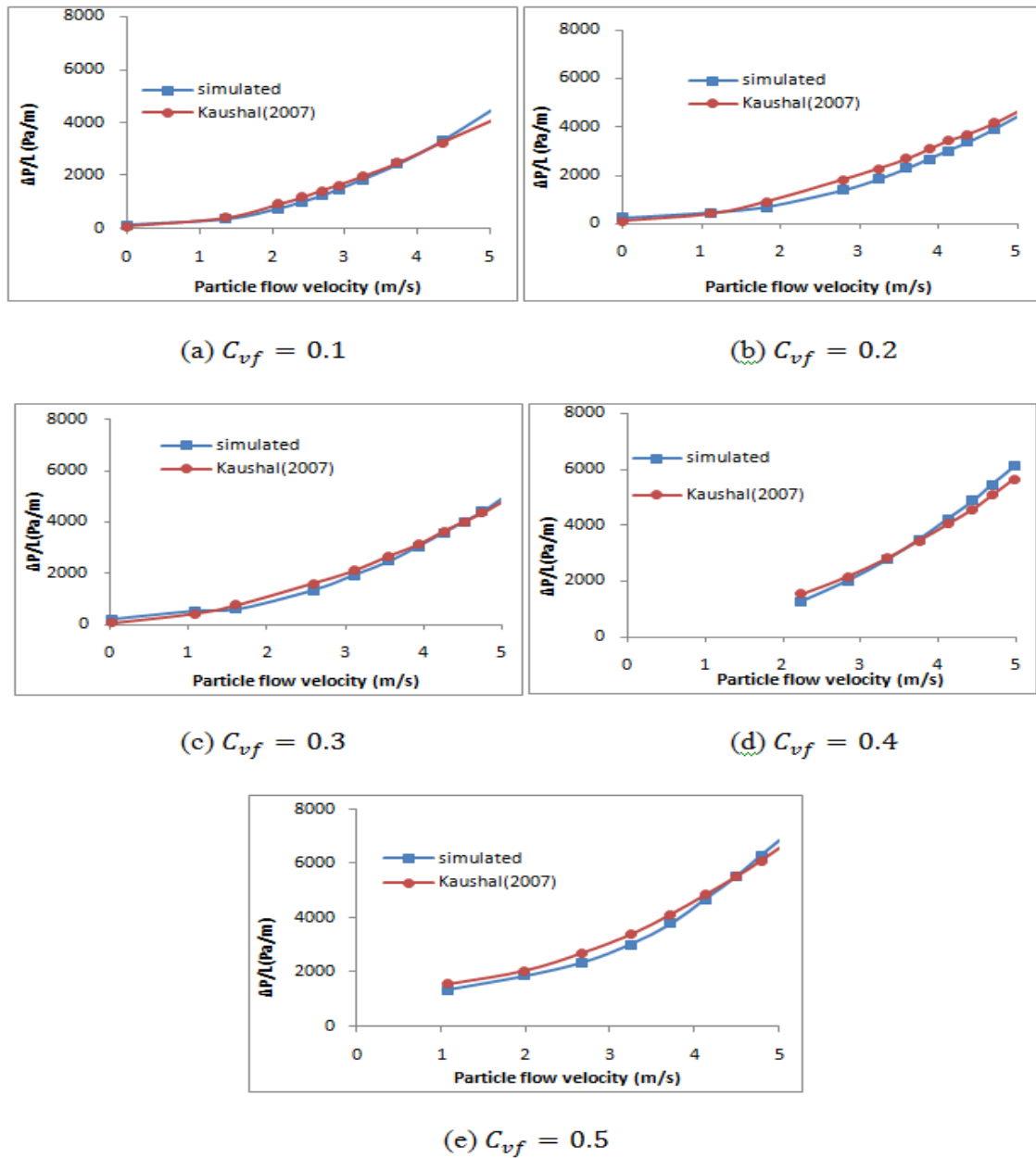


Figure 24. Comparison of simulated and experimental pressure drop over particle flow velocity at different solid volumetric concentration

5. Conclusions

This current study presents a three-dimensional CFD investigation of two phase (glass beads-water) flow through 54.9 mm diameter and 4 m long horizontal pipe for mixture velocity range of 1m/s to 5 m/s and solid volumetric concentration range of 10% to 50% by volume with one particle size 0.125 mm and particle density of 2470 kg/m³. Two phase Eulerian model with granular version and RNG K-ε turbulence model was verified and adopted for the slurry flow. The particles were treated as mono-dispersed. The subsequent conclusions can be drawn based on the current work:

- The solid particles are asymmetrically distributed alongside the vertical plane of cross section of the pipe
- When the particle flow velocity and volumetric concentration is low the higher concentration region is established at the lower half portion of the pipe, where the solid particles seem to be settled at the pipe base.

- For a given concentration as the flow velocity increases the turbulence energy increases which causes a decrease in the asymmetric distribution of the particles and particles tend to suspend rather than settling down at the bottom.
- The contacts of solid particles with the wall of pipe become more vivid with raise in flow velocity.
- Allocation of the solid particles in the horizontal plane turns into more visible with the increase in flow velocity and solid volumetric concentration, concentration distribution along the horizontal plane becomes more symmetric with raise in solid volumetric concentration.
- At a given flow velocity the turbulence of flow enhances with the rise in solid volumetric concentration.
- Velocity distribution is asymmetrical in the lower portion of the pipe along a vertical plane. This is due to the difference in density between the two phase and

because the solid particles are likely to accumulate at the base of the pipe.

- With the rise in flow velocity at a given solid volumetric concentration the velocity distribution becomes more symmetric as the increased turbulence energy provides a proper mixing of the solid particles and fluid at higher velocities.
- At a given velocity as the solid volumetric concentration increases the velocity distribution becomes more asymmetric and velocity increases as there is a rise in turbulence in the flow.
- The effect of solid volumetric concentration on pressure drop is such that pressure drop enhances with the rise in volumetric concentrations.
- The effect of turbulence on pressure drop shows that the pressure drop rises with the rise in turbulence for each level of solid volumetric concentration.

A mathematical correlation among pressure drop, turbulence and solid volumetric concentration is proposed which is developed from the simulated results. Calculated pressure drop using this proposed model illustrated an excellent concurrence with the experimental data. The obtained results of predetermined pressure drop are observed to be in synchronism with the experiment results. Moreover, the comparison of the simulated results proves the practical utility of proposed model, and high designing capability of Eulerian-Eulerian model with RNG $k-\epsilon$ turbulence model.

References

- [1] Seshadri, V., Malhotra, R.C., Sundar, K.S. Concentration and size distribution of solids in a slurry pipeline. In: Proc. 11th Nat. Conference on Fluid mechanics and fluid power, B.H.E.L., Hyderabad 1982.
- [2] Roco MC, Shook CA. Modeling of slurry flow: the effect of particle size. The Canadian Journal of Chemical Engineering. 1983;61(4):494-503.
- [3] Roco MC, Shook CA. Computational method for coal slurry pipelines with heterogeneous size distribution. Powder Technology. 1984;39(2):159-76.
- [4] Gillies RG, Shook CA, Wilson KC. An improved two layer model for horizontal slurry pipeline flow. The Canadian Journal of Chemical Engineering. 1991; 69(1):173-8.
- [5] Gillies RG, Shook CA, Xu J. Modeling heterogeneous slurry flows at high velocities. The Canadian Journal of Chemical Engineering. 2004;82(5):1060-5.
- [6] Doron P, Bamea D. Pressure drop and limit deposit velocity for solid-liquid flow in pipes. Chemical engineering science. 1995;50(10):1595-604.
- [7] Mukhtar A, Singh SN, Seshadri V. Pressure drop in a long radius 90° horizontal bend for the flow of multisized heterogeneous slurries. International journal of multiphase flow. 1995; 21(2):329-34.
- [8] Bellas J, Chaer I, Tassou SA. Heat transfer and pressure drop of ice slurries in plate heat exchangers. Applied Thermal Engineering. 2002; 22(7):721-32.
- [9] Matousek V. Pressure drops and flow patterns in sand-mixture pipes. Experimental thermal and fluid science. 2002; 26(6-7):693-702.
- [10] Scott SH, Abt SR. Hydraulic transport of fine and coarse sediment mixtures in pipelines. Journal of transportation engineering. 2002; 128(1):1-8.
- [11] Lahiri SK, Ghanta KC. Prediction of pressure drop of slurry flow in pipeline by hybrid support vector regression and genetic algorithm model. Chinese Journal of Chemical Engineering. 2008; 16(6):841-8.
- [12] Lahiri SK, Ghanta KC. Regime identification of slurry transport in pipelines: A novel modeling approach using ANN & differential evolution. Chemical Industry and Chemical Engineering Quarterly. 2010;16(4):329-43.
- [13] Chandel S, Singh SN, Seshadri V. Transportation of high concentration coal ash slurries through pipelines. International archive of applied sciences and technology. 2010; 1:1-9.
- [14] Kaushal DR, Kumar A, Tomita Y, Kuchii S, Tsukamoto H. Flow of mono-dispersed particles through horizontal bend. International Journal of Multiphase Flow. 2013; 52:71-91.
- [15] Nabil T, El-Sawaf I, El-Nahhas K. Computational fluid dynamics simulation of the solid-liquid slurry flow in a pipeline. InProc. 17th International Water Technologies Conference IWTC17 2013 (Vol. 57).
- [16] Kumar, U., Singh, S. N., & Seshadri, V. experimental investigation on pressure drop characteristics of bi-modal slurry flow in a straight horizontal PIPE, International Journal of Scientific and Engineering Research, 2015; 11(6), 153-158.
- [17] Kumar A. CFD Modeling for Slurry Flow Through Bends and Straight Pipe Line. InCAD/CAM, Robotics and Factories of the Future 2016 (pp. 615-623). Springer, New Delhi.
- [18] Gopaliya MK, Kaushal DR. Modeling of sand-water slurry flow through horizontal pipe using CFD. Journal of Hydrology and Hydromechanics. 2016; 64(3):261-72.
- [19] Kaushal DR, Tomita Y. Experimental investigation for near-wall lift of coarser particles in slurry pipeline using γ -ray densitometer. Powder Technology. 2007; 172(3):177-87.
- [20] Arora R, Arora R. Multiobjective optimization and analytical comparison of single- and 2-stage (series/parallel) thermoelectric heat pumps. International Journal of Energy Research. 2018; 42(4):1760-1778. <https://doi.org/10.1002/er.3988>
- [21] Arora R, Arora R. Multicriteria optimization based comprehensive comparative analyses of single-and two-stage (series/parallel) thermoelectric generators including the influence of Thomson effect. Journal of Renewable and Sustainable Energy. 2018; 10(4): pp.044701.
- [22] Arora R, Kaushik SC, Arora R. Multi-objective and multi-parameter optimization of two-stage thermoelectric generator in electrically series and parallel configurations through NSGA-II. Energy. 2015; 91: 242-254.
- [23] Arora R, Kaushik SC, Arora R. Thermodynamic modeling and multi-objective optimization of two-stage thermoelectric generator in electrically series and parallel configurations. Applied Thermal Engineering. 2016; 25(103): 1312-1323.
- [24] Arora R, Kaushik SC, Kumar R. Multi-objective thermodynamic optimization of solar parabolic dish Stirling heat engine with regenerative losses using NSGA-II and decision making. Applied Solar Energy. 2016; 52(4): 295-304.
- [25] Arora R, Kaushik SC, Kumar R, Arora R. Multi-objective thermo-economic optimization of solar parabolic dish Stirling heat engine with regenerative losses using NSGA-II and decision making. International Journal of Electrical Power & Energy Systems. 2016; 74: 25-35.
- [26] Arora R, Kaushik SC, Kumar Raj, Arora R. Soft computing based multi-objective optimization of Brayton cycle power plant with isothermal heat addition using evolutionary algorithm and decision making. Applied Soft Computing. 2016; 46: 267-283.
- [27] Arora R, Kaushik SC, Kumar R. Multi-objective thermodynamic optimization of solar parabolic dish Stirling heat engine using NSGA-II and decision making. International Journal of Renewable Energy Technology. 2017; 8(1): 64-92.
- [28] Kaushik SC, Kumar R, Arora R. Thermo-economic optimization and parametric study of an irreversible Brayton

- heat engine cycle. *Journal of Thermal Engineering*. 2016; 2(4): 861-870.
- [29] Kumar R., Kaushik SC, Kumar Raj. Performance Analysis of an Irreversible Regenerative Brayton Cycle based on Ecological Optimization Criterion. *International Journal of Thermal and Environment Engineering*. 2015; 9(1): 25-32.
- [30] Kumar R, Kaushik SC, Kumar R. Performance optimization of Brayton heat engine at maximum efficient power using temperature dependent specific heat of working fluid. *Journal of Thermal Engineering*. 2015; 1(2): 345-354.
- [31] Kumar R, Kaushik SC, Kumar R. Power optimization of an Irreversible regenerative Brayton Cycle using isothermal heat addition. *Journal of Thermal Engineering*. 2015; 1(4): 279-286.
- [32] Kumar R, Kaushik SC, Kumar Raj, Hans R. Multi-objective thermodynamic optimization of irreversible regenerative Brayton cycle using evolutionary algorithm and decision making. *Ain Shams Engineering Journal*. 2016; 7(2): 741-753.
- [33] Chiteka K, Arora R, Jain V. CFD prediction of dust deposition and installation parametric optimisation for fouling mitigation in non-tracking solar PVmodules. *International Journal of Ambient Energy*. 2019; pp.1-36 <https://doi.org/10.1080/01430750.2019.1594373>
- [34] Ahmed S, Arora R. Optimization of turning parameters of Aluminum 6351 T6 using Taguchi decision making technique. *International Journal of Data and Network Science*. 2017; 1(2): 27-38.
- [35] Ahmed SU, Arora R. Quality characteristics optimization in CNC end milling of A36 K02600 using Taguchi's approach coupled with artificial neural network and genetic algorithm. *International Journal of System Assurance Engineering and Management*. 2019. pp.1-20
- [36] Maputi ES, Arora R. Design optimization of a three-stage transmission using advanced optimization techniques. *International Journal for Simulation and Multidisciplinary Design Optimization*. 2019; 10: p.A8
- [37] Arora R, Arora R. Performance Characteristics and Thermodynamic Investigations on Single-Stage Thermoelectric Generator and Heat Pump Systems. *Pertanika Journal of Science & Technology*. 2018; 26(4): 1975-19